Tearing of Indian mantle lithosphere from high-resolution seismic images and its implications for lithosphere coupling in southern Tibet

Jiangtao Li[a] and Xiaodong Song[a,b,1]

[a]Department of Geology, University of Illinois at Urbana–Champaign, Champaign, IL 61820; and [b]School of Geodesy and Geomatics, Wuhan University, Wuhan 430079, China

Edited by Zhigang Peng, Georgia Institute of Technology, Atlanta, GA, and accepted by Editorial Board Member Lisa Tauxe July 3, 2018 (received for review October 5, 2017)

What happened to the Indian mantle lithosphere (IML) during the Indian–Eurasian collision and what role it has played on the plateau growth are fundamental questions that remain unanswered. Here, we show clear images of the IML from high-resolution P and S tomography, which suggest that the subducted IML is torn into at least four pieces with different angles and northern limits, shallower and extending further in the west and east sides while steeper in the middle. Intermediate-depth earthquakes in the lower crust and mantle are located almost exclusively in the high-velocity (and presumably strong) part of the Indian lithosphere. The tearing of the IML provides a unified mechanism for Late Miocene and Quaternary rifting, current crustal deformation, and intermediate-depth earthquakes in the southern and central Tibetan Plateau and suggests that the deformations of the crust and the mantle lithosphere are strongly coupled.

Tibetan Plateau | Indian mantle lithosphere | Pn tomography | continental deformation | tearing

Uplift of the Tibetan Plateau (TP) (Fig. 1), the largest and highest plateau in the world, is caused by the Cenozoic Indian–Eurasian collision (1, 2). However, what happens to the Indian mantle lithosphere (IML) during this process remains unclear. It has been proposed to be underthrusting or subducting beneath the southern and central TP (3–7). Moreover, seismic (4, 8–12) and geochemical (13) observations have suggested that the IML is possibly fragmented in certain locations.

Southern Tibet is characterized by thrust faults along the collisional front and a series of surface rifts with different ages in the northern Himalaya and Lhasa blocks (14) (see Fig. 1 for main boundaries and rifts). Normal-faulting earthquakes occur throughout the TP but are more common in south-central Tibet (Fig. 1). The dominant stress field in the TP changed from north–south shortening to east–west extension in Late Neogene (about 10 Ma) (15–17) to Quaternary, which has generally been attributed to gravitational potential energy of the thickened crust (18) but could have also involved mantle lithosphere (19). Equally unusual is the presence of normal-fault earthquakes under the Himalaya and TP at intermediate depth (70–110 km) (Fig. 1) (20, 21). Such intermediate-depth intracontinental earthquakes have been taken as an indication of a strong continental mantle lithosphere to accumulate elastic strain (20), a long-held view that has recently been challenged and debated (21–24). Here, we show clear images of the IML from high-resolution P and S tomography, which reveal a strong relationship between the IML and rifting, intermediate-depth earthquakes, and other observations in the southern TP.

Methods and Data

Our P and S images came from Pn tomography (*SI Appendix, Data and Methods for Pn Tomography*) and a recent surface-wave tomographic model (10), respectively. The Pn wave is a P wave traveling along the topmost mantle as the result of the sudden velocity increase at the Moho discontinuity and can be observed from ~200 to over 1,000 km in distance. The nature of the Pn wave turns a normally 3D tomography problem into a 2D problem for the topmost mantle, improving its lateral coverage and resolution. We used a large collection of Pn travel time data in Tibet from various sources (*SI Appendix, Data and Methods for Pn Tomography*). In particular, we included a dataset that consists of a large number of hand-picked Pn arrivals from temporary deployments (*SI Appendix*, Fig. S1), which improved significantly the coverage of the TP.

Results

The tomographic inversion shows that the Pn velocity is low in the north and high in the south in general (Fig. 2), consistent with previous studies (4, 25). We interpret the boundary between the north and the south from the improved image as the northern frontier of the IML (IML-F). The improved image also shows considerable complexities in the southern and central TP. The high-velocity regions are dissected by three narrow low-velocity bands that have a similar spacing and are nearly perpendicular to the collisional front. The strongest low-velocity anomaly along the Yadong–Gulu rift (YGR) was observed in a previous Pn tomography (4) and was interpreted as a tear of the IML (4, 9–11). The latest Pn image suggests that the IML has been torn into four main pieces with three dissecting tears or weak zones. Resolution and error analyses suggest that the high/low-velocity contrasts are resolvable and statistically robust (*SI Appendix*). We have also performed an anisotropic Pn tomography by including anisotropy in the Pn velocity (*SI Appendix*). The pattern of Pn velocity is quite

Significance

We show high-resolution P and S images of the subducted Indian mantle lithosphere, which has been torn into four main pieces. The tearing provides a unified mechanism for (*i*) Late Miocene and Quaternary rifting, (*ii*) mantle earthquakes in southern and central Tibet, and (*iii*) patterns of current crustal deformation (seismicity and GPS strain rate). It suggests (*iv*) that the deformations of the crust and the mantle lithosphere in southern Tibet are strongly coupled and thus we need to take a "deeper view" to understand the Himalayan–Tibetan continental deformation and evolution. The geometry of the Indian mantle lithosphere and the above issues are of fundamental importance and have been debated for decades. The proposed model has implications across geoscience disciplines.

Author contributions: J.L. and X.S. designed research; J.L. and X.S. performed research; J.L. and X.S. contributed new reagents/analytic tools; J.L. and X.S. analyzed data; and X.S. wrote the paper with contributions from J.L.

The authors declare no conflict of interest.

This article is a PNAS Direct Submission. Z.P. is a guest editor invited by the Editorial Board.

[1]To whom correspondence should be addressed. Email: xiao.d.song@gmail.com.

This article contains supporting information online at www.pnas.org/lookup/suppl/doi:10.1073/pnas.1717258115/-/DCSupplemental.

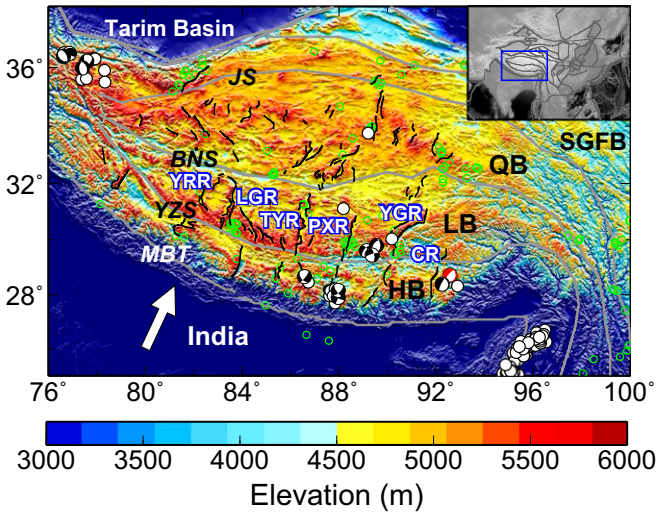

Fig. 1. Background topographic map (color) of the study region. *Inset* shows its location (blue box) in East and South Asia with topography (gray). The lines are the major block boundaries (gray) and rifts (normal faults) (14, 48) inside the TP (black line segments), respectively. The arrow indicates the Indian plate motion. The green circles are moderate and large normal-faulting earthquakes from Global Centroid–Moment–Tensor catalog (ref. 49; Mw ≥ 5 from 1976 to 2016), the white circles are intermediate-depth earthquakes (depth, ≥70 km) from the relocated EHB catalog (ref. 33; 1960–2008), and the focal mechanisms are high-quality (HQ) intermediate-depth earthquakes (depth, ≥70 km) determined from individual studies and listed in refs. 20 (black) and 34 (red). BNS, Bangong–Nujiang suture; CR, Comei rift; HB, Himalaya block; JS, Jinsha suture; LB, Lhasa block; LGR, Lunggar rift; MBT, Main Boundary Thrust; PXR, Pumqu–Xianza rift; QB, Qiangtang block; SGFB, Songpan–Ganzi fold belt; TYR, Tangra Yum Co rift; YGR, Yadong–Gulu rift; YRR, Yari rift; YZS, Yarlung–Zangbu suture.

similar to the inversion without including the Pn anisotropy, suggesting the Pn velocity pattern is not significantly affected by the anisotropy (*SI Appendix*, Fig. S4).

Our recent high-resolution S-wave model from surface-wave (Rayleigh-wave) tomography (10) (Fig. 3) agrees with the Pn results. The 3D S-wave images show clearly high velocities separated by low-velocity bands in the top part of the mantle in the map view (Fig. 3*A* and *SI Appendix*, Fig. S6*A*), in the depth view (Fig. 3*B*), and in the 3D view (*SI Appendix*, Fig. S6*B*). The slow Pn and the slow S anomalies are at similar but are not exactly at the same locations. The location of T1 is nearly the same, but the location of T2 or T3 can differ by 1–2°. The discrepancy may be caused for the following reasons. First, Pn and surface waves have different sensitivities. The surface wave is sensitive to the average velocity profile with depth, while the Pn wave is sensitive to the very top of the mantle. Because of the vertical averaging of surface wave data, it is not meaningful to examine the S-velocity map right below the Moho. Second, the slow-velocity structures may not be vertical, thus appearing at slightly different locations at different depths (*SI Appendix*, Fig. S6*A*). Third, the P and S tomographic resolutions are different. The Pn and surface-wave datasets are independent, giving rise to different resolutions. Furthermore, the resolutions are still limited because of the limited station coverage, particularly in the western TP.

Combining the Pn image and the 3D S model (Figs. 2 and 3 and *SI Appendix*, Figs. S5 and S6), we infer the geometry of the IML as follows. The IML has been fragmented into four segments, which have different advancements and subduction angles. The segment in the east (S1) shows nearly flat subduction and advanced the most to about the Jinsha suture; the segment in the west (S4) is also flat, advancing to the Tarim Basin; and the segments in the middle (S2 and S3) have steeper subduction and advanced to about the Bangong–Nujiang suture with S2 perhaps even steeper than S3.

The 3D S model above is not deep enough to constrain the bottom of the IML. However, the lithosphere–asthenosphere boundary is imaged along a few dense north-south seismic profiles in S4, S3, S2 (and T1) (7, 26), and the IML geometry is consistent with our results with an increasing angle of subduction from S4 to S2 (7). Recent P tomography (27) shows clear fast–slow along-strike variations extending to depths of at least 260 km. Fast velocities extend further north in the western (S4) and eastern (S1) parts of the TP. T1 and T2 can be seen in an enlarged view of 100-km depth at longitudes of 90 and 85°, respectively. T3 does not seem to show up in their model, whose resolution may be limited by sparse station distribution in the western TP. Alternating fast–slow anomalies can also be observed from teleseismic P and S tomography under the eastern part of the TP from ref. 28. A band of low velocities are observed in T1 down to depth of 250 km in both their P and S models. Results from recent adjoint waveform tomography (29, 30) also show similar fast–slow along-strike pattern in the uppermost mantle of the TP when we zoom in. Chen et al. (30) observed low-velocity anomalies at depths shallower than 150 km, suggesting possible partial melting. However, they did not observe large-scale low-velocity anomalies at greater depths, although the low resolution in their studies with sparse station distribution in central-western TP may underestimate the level of the lateral heterogeneities and may not resolve the relatively fine-scale low-velocity bands at these depths.

The presence of the IML and its influence on the mantle flow in the asthenosphere are likely to affect the shear-wave (SKS) splitting pattern, which have been reported previously along a few linear profiles (7, 11, 26, 31). We compared a large collection of SKS splitting measurements (32) with the S model in the

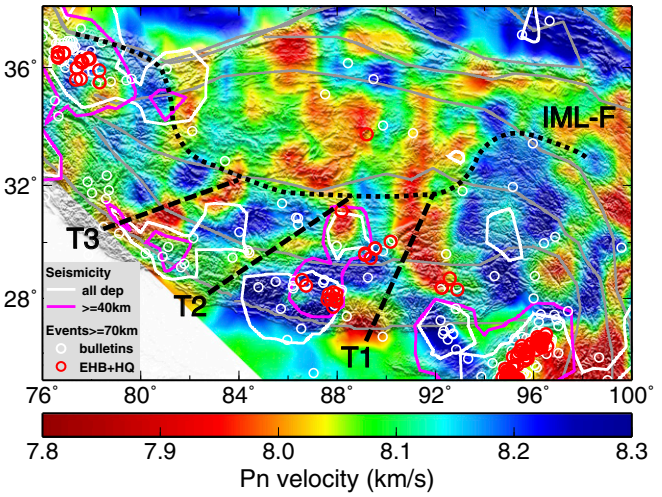

Fig. 2. Map of Pn velocity (color) and seismicity (symbols and contours). The block boundaries (gray lines) are the same as in Fig. 1. The circles indicate intermediate-depth earthquakes (≥70 km): the relocated intermediate-depth events (red circles) from the EHB catalog and the high-quality (HQ) determinations (Fig. 1) and routine earthquake bulletins (magnitude of ≥4.5 from 1960 to 2017) (white circles) from the International Seismological Centre (ISC), the US Geological Survey Preliminary Determination of Earthquakes, and the China Earthquake Administration. The thick white (or magenta) contours indicate earthquake clusters where the number of earthquakes of all depths (or depth ≥ 40 km) within a 1-by-1° cell is larger than 190 (or 50), calculated using the ISC catalog (1960–2017, magnitude ≥ 4.0) (*SI Appendix*, Fig. S9). The black dashed lines denote the locations of the three possible tears of the IML, and the black dotted line marks the approximate location of the northern frontier of the IML (IML-F). We cut off the bottom-left corner of lower resolution (*SI Appendix*, Fig. S2).

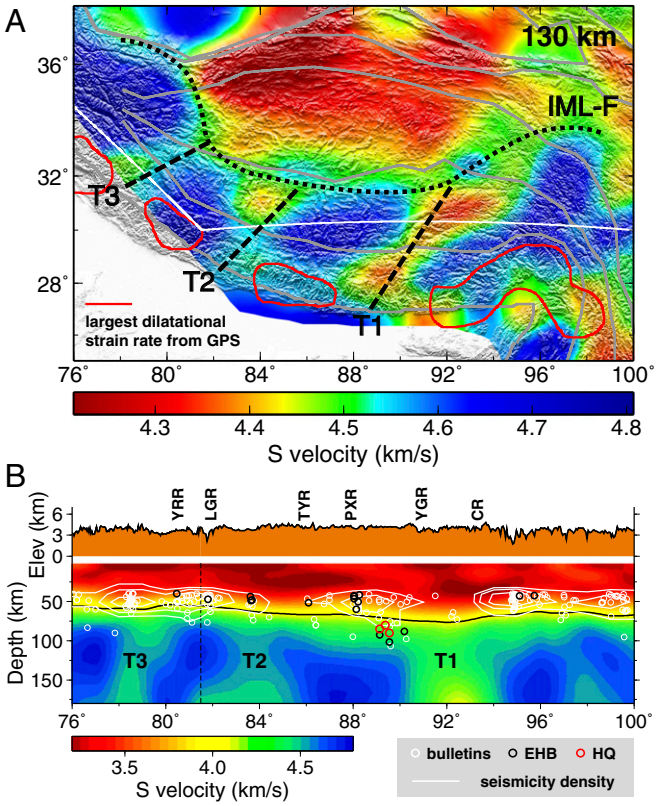

Fig. 3. Comparisons of S-velocity images (color) from surface-wave tomography (10) and other geophysical observations. (*A*) S-velocity map at 130-km depth. The red contours indicate areas of the largest dilatational strain rates of less than −50 nanostrain/y, calculated from GPS measurements with a smaller smoothing constant by ref. 36, which display four localized strong compression areas along the collisional front. The black dashed lines denote the locations of the three possible tears of the IML, and the black dotted line marks the approximate location of the IML-F. The locations are similar to those in Fig. 2. The bottom-left edge is cut according to the resolution in ref. 10. (*B*) S-velocity cross-section along the white line in *A*. The elevation and the approximate locations of surface rifts are shown on *Top* (see Fig. 1 for abbreviations). The dashed line marks the turning point of the white line in *A*. The solid line shows the Moho estimated using the method by ref. 50. The circles are earthquakes deeper than 40 km within ±1° of the profile from the routine bulletins (white; magnitude, ≥4.5; 1960–2017), the EHB bulletin (black), and the high-quality (HQ) determinations (red). The white contours show where there are more than 4, 10, and 20 bulletin earthquakes, respectively, within ±1° in longitude and ±10 km in depth. The three tears of the IML are marked (T1 to T3).

mantle (*SI Appendix*, Fig. S7). We see changes of the splitting pattern across the IML-F line. In the northern TP in the Qiangtang block, the delay times are generally larger than 1.5 s or even 2.0 s and the fast directions are mostly in the east–west direction, which correlates with the large area of low velocities in the mantle and suggests a strong eastward mantle flow. South of the IML-F, however, the delay times are mostly smaller than 1.0 s and the null stations (with no measurable splitting) are located almost exclusively in high-velocity regions, which may be due to the presence of the thick IML. Both the delay times and the fast directions are much more variable with many parallel to the slab-tear directions or oblique to the fast directions in the north, which may be attributed to the influence of the complex geometry of the IML with segmentation and different angles of underthrusting.

The locations of the unusually intermediate-depth intracontinental earthquakes in the southern TP show a striking correlation with the fragmented IML (Figs. 2 and 3*B* and *SI Appendix*, Fig. S5). The earthquakes are located in the high P velocities within the mantle lid (Pn velocities) with very few exceptions (Fig. 2), including events from routine bulletins and relocated events (depth, ≥70 km). The focal depths in bulletins have significant errors. However, statistical analyses on the depth distribution (*SI Appendix*, Fig. S8) of the moderate-size earthquakes (magnitude, ≥4.5) relative to the fast velocities of the IML (Fig. 3*B* and *SI Appendix*, Fig. S5) suggest that the probability that all of the intermediate-depth earthquakes are in the crust is extremely small, that is, some of them must be in the IML as indicated by relocated events (below). The intermediate-depth events (depth, ≥70 km) from the Engdahl–van der Hilst–Buland (EHB) bulletins (33), which have been relocated using depth phases, are all in the IML (Fig. 3*B* and *SI Appendix*, Fig. S5; with only one exception in the northern TP). Some selected events, which we refer as high-quality events, have been carefully relocated using waveforms that are listed in refs. 21 and 34, including three that must be from the mantle according to waveform characteristics (35). Intermediate-depth high-quality events (depth, ≥70 km) are located exclusively in the fast regions in southeast Tibet (Himalaya and the southern TP) and northwest Tibet (the western Kunlun) (Figs. 1 and 2), respectively. We thus conclude that at least some of intermediate-depth events in Himalaya, south Tibet, and western Kunlun are in the mantle and that these mantle earthquakes are associated with the cold (fast) parts of the subducted IML. The low occurrence of intermediate-depth earthquakes along the three tears, particularly the seismicity gap under the YGR (T1), is consistent with the IML having been weakened by a lithospheric tear.

The high-quality intermediate-depth events in southeast and northwest Tibet have focal mechanisms consistent with east–west extension, similar to active extension and faulting at the shallow crust throughout the southern and central Tibet (Fig. 1). The observation has been used to argue against the Indian subduction as the cause of the intermediate-depth earthquakes (21); however, the tearing of the IML would be consistent with the significant normal faulting component of the intermediate-depth events under the TP.

Crustal seismicity and surface deformation also show a regular pattern that correlates well with the inferred fragmented IML (Figs. 2 and 3), which seems to suggest strong coupling between the mantle lithosphere and crustal and surface deformation. The focal mechanisms in the southern and central TP are dominated by normal and strike-slipping faulting and so are the intermediate-depth earthquakes. The distribution of earthquakes in the upper crust or in the lower crust shows patches of most active seismicity (*SI Appendix*, Fig. S9) that coincide with fast mantle velocity blocks (Fig. 2). Most seismicity (at the upper crust, lower crust, or the mantle) is separated by three noticeable gaps that coincide with the P and S low-velocity bands in mantle lid (Figs. 2 and 3*B* and *SI Appendix*, Fig. S5*A*). The most striking example is in the vicinity of the YGR, which shows low seismicity at all depths and low velocities in the mantle and midcrust (Figs. 2 and 3 and *SI Appendix*, Fig. S5*A*).

A most recent strain rate calculation with good GPS station coverage in southern Tibet (36) displayed a very clear pattern of four strong localized compression segments along the collisional front when little smoothing was used (Fig. 3*A*). The four contours of strongest compression (with the largest dilatational strains less than −50 nanostrain/y) fall in the four segments outlined by the high mantle lithosphere velocities. This observation indicates strong coupling of the IML and the shallow crust, producing the stronger localized compression at the collisional front. On the other hand, in the bands where there are tears and perhaps local upwelling in the tears, the subduction would exert considerably weaker mechanical coupling, resulting in a weaker compression at the collisional front.

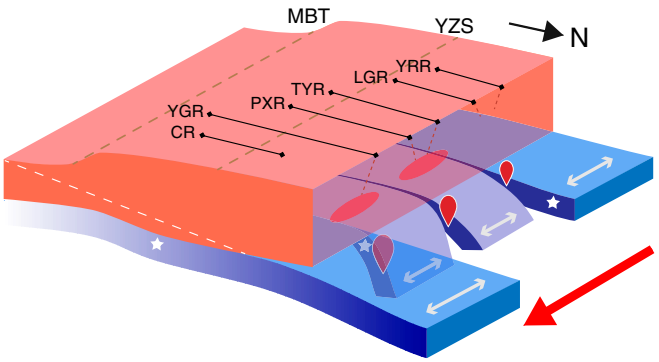

Fig. 4. Idealized cartoon illustration of the tearing of the IML and coupling between the crust (orange) and the mantle lithosphere (blue) in south-central Tibet. The thickness of the crust and mantle lithosphere is not to scale. The white dashed line marks the possible boundary between the underthrusting Indian crust and the overriding Himalayan orogenic prism (south of YZS) and Tibetan crust (south of YZS) with reference to ref. 6. The simplified block boundaries and rifts are shown on the surface (see Fig. 1 for the abbreviations). The underthrusting IML is flatter and advances further in the west and east. The tearing of the IML from nonuniform advancement results in extension (white arrows) and normal-faulting intermediate-depth earthquakes (stars). The extensional stress couples to the crust and result in extension and rifting in the upper crust. The IML tears may not be uniform with the tear under YGR the strongest and they may not have one-to-one relationship with surface rifts. The IML tearing may induce local mantle upwelling (red blobs) and the increased temperature at depth may produce midcrust low-velocity zones (red lenses), which may connect to the surface rifts (dashed brown lines). The large red arrow implies eastward mantle flow in northern Tibet.

A Conceptual Model

The several different types of geophysical observations above (mantle P and S velocities, SKS splitting, mantle and crustal seismicity, focal mechanisms, and surface strain rate) seem to point to a consistent picture (Fig. 4) that the IML has been torn into four main segments (S1 to S4) with three main tears (T1 to T3) (Figs. 2 and 3 and *SI Appendix*, Figs. S5 and S6) and that the geometry of the subducted IML is likely to exert strong influence on the mantle flow of the TP as well as the deformation of the entire crust of the southern and central TP. The elevated topography in the TP alone may not have sufficient gravitational potential energy to produce east–west extension under the influence of compressive stresses at the convergence boundary (37). The rapid rise of the TP from the convective removal of the thickened mantle lithosphere may produce sufficient east–west extension to replace the north–south compression as the dominant feature of the TP (38), which may explain the rifting and normal faulting in the northern and central TP. However, much of the IML in the southern and part of the central TP has remained (Fig. 2 and *SI Appendix*, Figs. S5 and S6). We propose that the IML tearing may be the main cause of the crustal extension, rifting, and melting in the south-central TP. The frontier of the IML may have met different resistance along the strike, advancing shorter distance and at a steeper angle in the middle due to stronger Lhasa block (39, 40) and further at a shallow dip in the east and in the west. The heterogeneous resistance and advancement caused the IML to tear, which caused extension in the coupled crust and lithosphere (41) and multiple rifts in brittle upper crust but might not involve asthenosphere upwelling at greater depths (30). The lithosphere tearing or weakening is not uniform, with T1 much more prominent than T2 and T3. The lithospheric tears (weak zones) do not have one-to-one correspondence with surface rifts as the heterogeneous upper crust responds to stress field from the mantle lithosphere, convergent boundary, and surface loading.

The lithosphere tearing may be facilitated by preexisting weak zones of the Indian plate that are deep-seated to at least lower crust (42). In fact, gravity data traced three Indian basement ridges (Munger–Saharsa ridge, Faizabad ridge, and Delhi–Hardwar ridge from east to west) to the vicinities of T1–T3, respectively, underneath the Himalayas and the southern Tibet (42). Large earthquakes of the past millennium (43) were found within segments of the Himalayan collision zone, which did not propagate across the segment boundaries of the inherited structure of the Indian plate (44). Considering the deep-seated weak zones and the segmentations of the present-day strain at surface (Fig. 3) and the lithosphere structure at depth (this study), we concur with the recent proposal (44) that the lateral extent of potential megathrust earthquakes may be limited by the segment boundaries. Our model of IML tearing is consistent with other geological and geochemical observations. Mechanical arguments on the large rift spacing in the TP suggest that that east–west extension must have involved mantle lithosphere (19). The model can explain asynchronous volcanism that preceded the initiation of rifts in southern Tibet (45). It is also consistent with a mantle source of the observed ultrapotassic adakites in southern Tibet (46) and a large area of the negative aeromagnetic anomaly (47) in the central segments, presumably a result of demagnetization from mantle heat flow (13).

ACKNOWLEDGMENTS. Critical and insightful reviews from the reviewers and the editor helped improve the manuscript greatly. The bulletin data were from the International Seismological Centre, the US Geological Survey, and the China Earthquake Administration. The digital seismograms of the temporary stations for the new Pn picks were from the Data Management Center of the Incorporated Research Institutions for Seismology. We thank Min Chen for sharing their adjoint tomography model with us. This research was supported by the National Science Foundation (Grant EAR 1620595), the China National Special Fund for Earthquake Scientific Research in Public Interest (Grant 201508020), and the National Natural Science Foundation of China (Grant 41774056).

1. Molnar P, Tapponnier P (1975) Cenozoic tectonics of Asia: Effects of a continental collision: Features of recent continental tectonics in Asia can be interpreted as results of the India-Eurasia collision. *Science* 189:419–426.
2. Yin A, Harrison TM (2000) Geological evolution of the Himalayan-Tibetan orogen. *Annu Rev Earth Planet Sci* 28:211–280.
3. Tilmann F, Ni J; INDEPTH III Seismic Team (2003) Seismic imaging of the downwelling Indian lithosphere beneath central Tibet. *Science* 300:1424–1427.
4. Liang C, Song X (2006) A low velocity belt beneath northern and eastern Tibetan Plateau from Pn tomography. *Geophys Res Lett* 33:L22306.
5. Li C, van der Hilst RD, Meltzer AS, Engdahl ER (2008) Subduction of the Indian lithosphere beneath the Tibetan Plateau and Burma. *Earth Planet Sci Lett* 274: 157–168.
6. Nábelek J, et al.; Hi-CLIMB Team (2009) Underplating in the Himalaya-Tibet collision zone revealed by the Hi-CLIMB experiment. *Science* 325:1371–1374.
7. Zhao J, et al. (2010) The boundary between the Indian and Asian tectonic plates below Tibet. *Proc Natl Acad Sci USA* 107:11229–11233.
8. Ceylan S, et al. (2012) Fragmented Indian plate and vertically coherent deformation beneath eastern Tibet. *J Geophys Res* 117:B11303.
9. Liang X, et al. (2012) A complex Tibetan upper mantle: A fragmented Indian slab and no south-verging subduction of Eurasian lithosphere. *Earth Planet Sci Lett* 333–334: 101–111.
10. Bao X, Song X, Li J (2015) High-resolution lithospheric structure beneath Mainland China from ambient noise and earthquake surface-wave tomography. *Earth Planet Sci Lett* 417:132–141.
11. Chen Y, Li W, Yuan X, Badal J, Teng J (2015) Tearing of the Indian lithospheric slab beneath southern Tibet revealed by SKS-wave measurements. *Earth Planet Sci Lett* 413:13–24.
12. Peng M, et al. (2016) Complex Indian subduction style with slab fragmentation beneath the eastern Himalayan syntaxis revealed by teleseismic P-wave tomography. *Tectonophysics* 667:77–86.
13. Hou Z-Q, Zhao Z-D, Gao Y-F, Yang Z-M, Jiang W (2006) Tearing and dischronal subduction of the Indian continental slab: Evidence from Cenozoic Gangdese volcano-magmatic rocks in south Tibet. *Acta Petrol Sin* 22:761–774.
14. Taylor MH, Yin A (2009) Active structures of the Himalayan-Tibetan orogen and their relationships to earthquake distribution, contemporary strain field, and Cenozoic volcanism. *Geosphere* 5:199–214.

15. Coleman ME, Hodges KV (1995) Evidence for Tibetan Plateau uplift before 14 Myr ago from a new minimum age for east-west extension. *Nature* 374:49–52.
16. Yin A, et al. (1999) Significant late Neogene east-west extension in northern Tibet. *Geology* 27:787–790.
17. Blisniuk PM, et al. (2001) Normal faulting in central Tibet since at least 13.5 Myr ago. *Nature* 412:628–632.
18. Molnar P, Tapponnier P (1978) Active tectonics of Tibet. *J Geophys Res* 83:5361–5375.
19. Yin A (2000) Mode of Cenozoic east-west extension in Tibet suggesting a common origin of rifts in Asia during the Indo-Asian collision. *J Geophys Res* 105:21745–21759.
20. Chen W-P, Molnar P (1983) Focal depths of intracontinental and intraplate earthquakes and their implications for the thermal and mechanical properties of the lithosphere. *J Geophys Res* 88:4183–4214.
21. Chen W-P, Yang Z (2004) Earthquakes beneath the Himalayas and Tibet: Evidence for strong lithospheric mantle. *Science* 304:1949–1952.
22. Maggi A, Jackson J, Priestley K, Baker C (2000) A re-assessment of focal depth distribution in southern Iran, the Tien Shan and northern India: Do earthquakes really occur in the continental mantle? *Geophys J Int* 143:629–661.
23. Jackson J (2002) Strength of the continental lithosphere: Time to abandon the jelly sandwich? *GSA Today* 12:4–10.
24. Priestley K, Jackson J, McKenzie D (2008) Lithospheric structure and deep earthquakes beneath India, the Himalaya and southern Tibet. *Geophys J Int* 172:345–362.
25. Liang C, Song X, Huang J (2004) Tomographic inversion of Pn travel times in China. *J Geophys Res* 109:B11304.
26. Kumar P, Yuan X, Kind R, Ni J (2006) Imaging the colliding Indian and Asian lithospheric plates beneath Tibet. *J Geophys Res* 111:B06308.
27. Wei W, Zhao D, Xu J, Zhou B, Shi Y (2016) Depth variations of P-wave azimuthal anisotropy beneath Mainland China. *Sci Rep* 6:29614.
28. Liang X, et al. (2016) 3D imaging of subducting and fragmenting Indian continental lithosphere beneath southern and central Tibet using body-wave finite-frequency tomography. *Earth Planet Sci Lett* 443:162–175.
29. Chen M, Niu F, Liu Q, Tromp J, Zheng X (2015) Multiparameter adjoint tomography of the crust and upper mantle beneath East Asia: 1. Model construction and comparisons. *J Geophys Res Solid Earth* 120:1762–1786.
30. Chen M, et al. (2017) Lithospheric foundering and underthrusting imaged beneath Tibet. *Nat Commun* 8:15659.
31. Chen W-P, et al. (2010) Shear-wave birefringence and current configuration of converging lithosphere under Tibet. *Earth Planet Sci Lett* 295:297–304.
32. Wüstefeld A, Bokelmann G, Barruol G, Montagner JP (2009) Identifying global seismic anisotropy patterns by correlating shear-wave splitting and surface waves data. *Phys Earth Planet Inter* 176:198–212.
33. Engdahl ER, van der Hilst RD, Bulland R (1998) Global teleseismic earthquake relocation with improved travel times and procedures for depth determination. *Bull Seismol Soc Am* 88:722–743.
34. Chu R, Zhu L, Helmberger DV (2009) Determination of earthquake focal depths and source time functions in central Asia using teleseismic P waveforms. *Geophys Res Lett* 36:L17317.
35. Zhu L, Helmberger DV (1996) Intermediate depth earthquakes beneath the India-Tibet collision. *Geophys Res Lett* 23:435–438.
36. Ge W-P, Molnar P, Shen Z-K, Li Q (2015) Present-day crustal thinning in the southern and northern Tibetan Plateau revealed by GPS measurements. *Geophys Res Lett* 42: 5227–5235.
37. England P, Houseman G (1986) Finite strain calculations of continental deformation: A comparison with the India-Asia collision zone. *J Geophys Res* 91:3664–3676.
38. England P, Houseman G (1989) Extension during continental convergence, with application to the Tibetan Plateau. *J Geophys Res* 94:17561–17579.
39. Murphy MA, et al. (1997) Did the Indo-Asian collision alone create the Tibetan Plateau? *Geology* 25:719–722.
40. Wang C, et al. (2008) Constraints on the early uplift history of the Tibetan Plateau. *Proc Natl Acad Sci USA* 105:4987–4992.
41. Copley A, Avouac JP, Wernicke BP (2011) Evidence for mechanical coupling and strong Indian lower crust beneath southern Tibet. *Nature* 472:79–81.
42. Godin L, Harris LB (2014) Tracking basement cross-strike discontinuities in the Indian crust beneath the Himalayan orogen using gravity data—relationship to upper crustal faults. *Geophys J Int* 198:198–215.
43. Bilham R, Gaur VK, Molnar P (2001) Earthquakes. Himalayan seismic hazard. *Science* 293:1442–1444.
44. Hetényi G, et al. (2016) Segmentation of the Himalayas as revealed by arc-parallel gravity anomalies. *Sci Rep* 6:33866.
45. Yin A, et al. (1994) Tertiary structural evolution of the Gangdese thrust system, southeastern Tibet. *J Geophys Res* 99:175–201.
46. Hou Z-Q, Gao Y-F, Qu X-M, Rui Z-Y, Mo X-X (2004) Origin of adakitic intrusive generated during mid-Miocene east-west extension in southern Tibet. *Earth Planet Sci Lett* 220:139–155.
47. He R, Gao R, Zheng H, Zhang J (2007) Match-filter analyzing areomagnetic anomaly in mid-western Tibetan Plateau and its tectonic implications. *Chin J Geophys* 50: 1131–1140.
48. Styron R, Taylor MH, Okoronkwo K (2010) HimaTibetMap-1.0: New "web-2.0" online database of active structures from the Indo-Asian collision. *Eos* 91:20.
49. Dziewonski AM, Chou T-A, Woodhouse JH (1981) Determination of earthquake source parameters from waveform data for studies of global and regional seismicity. *J Geophys Res* 86:2825–2852.
50. Xu Z, Song X, Zheng S (2013) Shear velocity structure of crust and uppermost mantle in China from surface wave tomography using ambient noise and earthquake data. *Earthquake Sci* 26:267–281.